Investigation of Cracking in 230 Ni Alloy Prepared by Direct Metal Laser Sintering

Kristen Adair, Mohsin Hasan, Xuanpu Ning, Bo Yang
Faculty Advisors: Dr. Xinghang Zhang
Industrial Sponsors: Bill Jarosinski, Jack Lopez
Acknowledgements: Jie Ding for assistance with SEM and EDS

Abstract: Ni Alloy 230, a commonly used aerospace alloy, often develops cracks during Direct Metal Laser Sintering. This project shows that cracks appear to be the least at an energy density of ~ 70 J/m^3. New composition with lower Si and Mn showed significantly reduced cracking and abundant γ' precipitates. The cracks may arise from grain boundary liquation along the γ' phase, or through thermal stress gradients induced intergranular cracking.

This work is sponsored by Praxair Surface Technologies, Indianapolis, IN

Project Background

Direct Metal Laser Sintering (DMLS) is an additive manufacturing method that is widely used to print a variety of Ni alloys. Figure 1 displays a schematics and several key parameters for printing. The parameters combine to define energy density widely used to compare printing conditions.

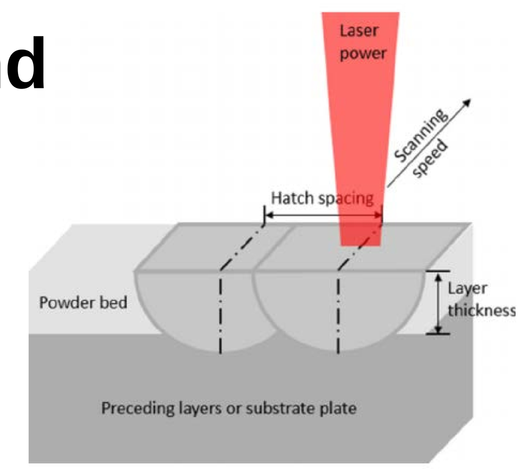

Figure 1: Schematic illustration of DMLS printing parameters.[1]

$$\psi = \frac{P}{v * d * h}$$

Energy Density - Ψ,
P - laser power,
v - scan speed,
h - layer thickness,
d - hatch spacing.

Alloy 230 is a commonly used aerospace alloy for high temperature sections of aircraft engines due to its extreme resistance to high-temperature creep and corrosion.

Table 1: Alloy 230 chemistries by weight percent of each element.

	Ni	Cr	W	Co	Fe	Mo	Mn	Si	C	B
Alloy 230	Bal	20-24	13-15	5	⩽3	1-3	0.3-1	0.35-0.75	0.15-0.005	⩽0.0015
Alloy 230 - A	Bal	21.54	14.27	0.11	0.14	2.01	0.004	0.25	0.0665	0.005
Alloy 230 - W	Bal	22	14	5	3		0.5	0.5	0.07	0.002
Alloy 230 - B	Bal	23.06	14.43	3.19	1.9	2.52		0.26	0.05	0.003
Alloy 230 - C	Bal	21.39	13.49	3.02	1.8	2.39		0.47	0.06	0.014

Alloy 230 – W

Table 2: Energy density for various printing parameters (Laser power 200 W)

Layer Thickness (μm)	40	1	2	3	4	5	
Hatch (μm)	Scan Speed (mm/s)	700	800	900	1000	1100	Plane
80	1	119J/cm^3	104.2J/cm^3	92.6J/cm^3	83.3J/cm^3	75.8J/cm^3	XZ
90	2	105.8J/cm^3	92.6J/cm^3	82.3J/cm^3	74.1J/cm^3	67.3J/cm^3	XY
90	2	105.5J/cm^3	92.6J/cm^3	82.3J/cm^3	74.1J/cm^3	67.3J/cm^3	YZ
100	3	95.2J/cm^3	83.3J/cm^3	74.1J/cm^3	66.7J/cm^3	60.6J/cm^3	XY

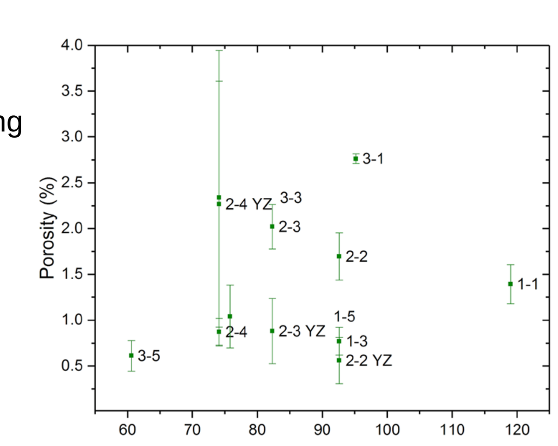

Figure 2: Porosity of alloy 230-W calculated from optical micrographs.

- The Alloy 230 - W composition used as weld filler
- The Alloy 230 - W exhibited uniformly distributed cracks
- Larger energy density is correlated to lead lower crack density.

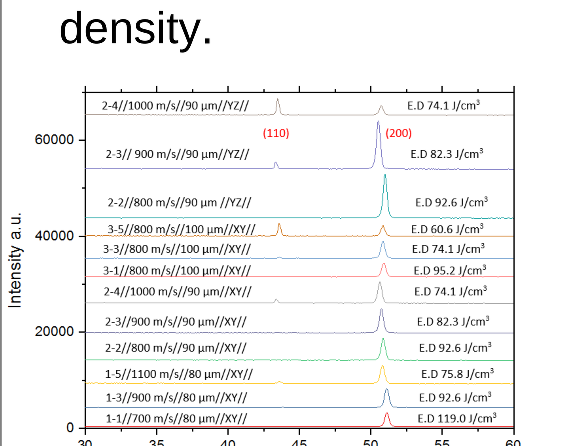

Figure 3: X-Ray Diffraction Pattern of 230 W sample

- 2 evident peaks: (111) and (200).
- The crack density does not show a strong correlation with the ratio between the intensity of (111) and (200).

- A smaller hatch spacing leads to a lower crack density.
- No obvious precipitates in the SEM images.
- EDS maps showed uniform distribution of Ni, Co, Cr, Mo, Al and B, and segregation of W near the crack.

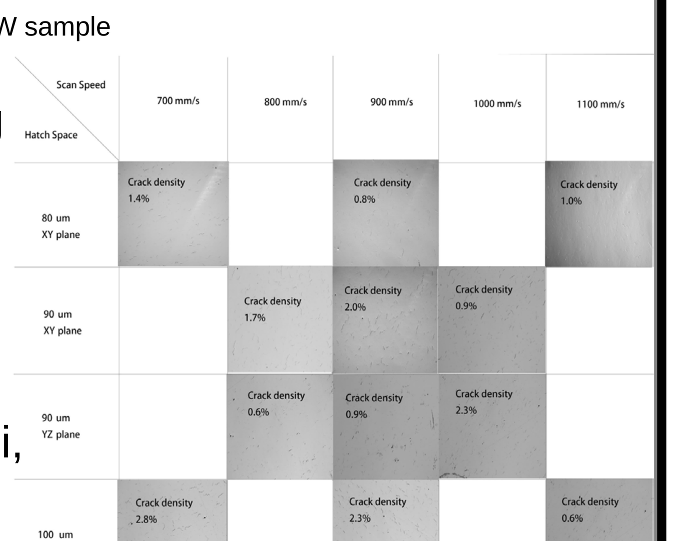

Figure 4: Optical Micrograph overview corresponding to parameter matrix of samples in Alloy 230 – W

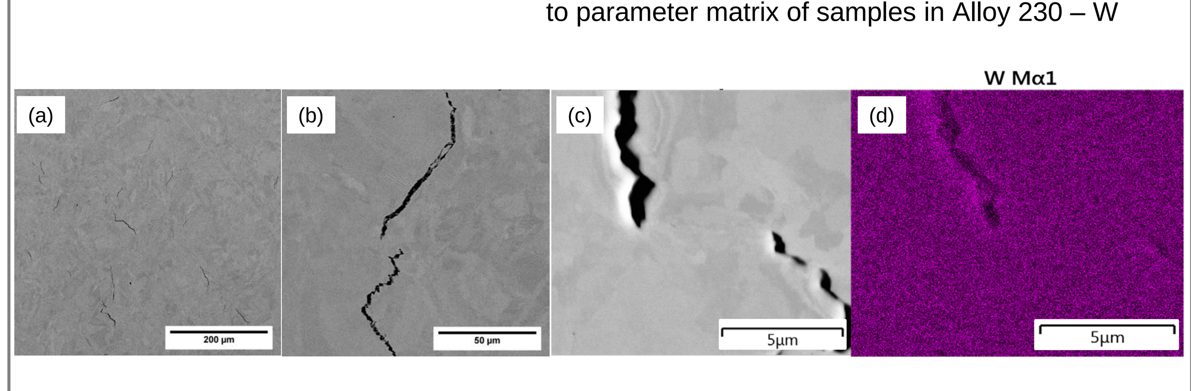

Figure 5: (a) SEM Images of the sample 2-3 at 500X; (b) SEM image showing the crack in sample 2-3 at 2000X; (c) SEM Image of the EDS mapping area; (d) The distribution of W in the matrix.

Methods

Porosity (Crack Density)

- Porosity quantitatively defines the amount of cracks in each sample.
- Optical/SEM images were used to calculate the porosity.

XRD

- XRD performed on a D8 Focus Bruker, 30° to 60°

Hardness

- Vickers test was performed on Leco LM247AT microhardness tester.

SEM

- SEM performed on Phenom Desktop SEM, Quanta 650 FEG, and FEI Quanta 3D FEG.

EDS

- Performed on FEI Quanta 3D FEG to analyze the distribution of elements in the specimens.

Alloy 230 - B

Table 3: Printing parameters and energy densities of alloy 230-B

Layer Thickness (μm)	30			1	2	3	4
Hatch (um)	100		Scan Speed (mm/s)	900	1000	1100	1200
Laser Power (W)		200	1	74.1J/cm^3	66.7J/cm^3	60.6J/cm^3	55.6J/cm^3
		250	2	92.6J/cm^3	83.3J/cm^3	75.8J/cm^3	69.4J/cm^3
		300	3	111.1J/cm^3	100J/cm^3	90.9J/cm^3	83.3J/cm^3

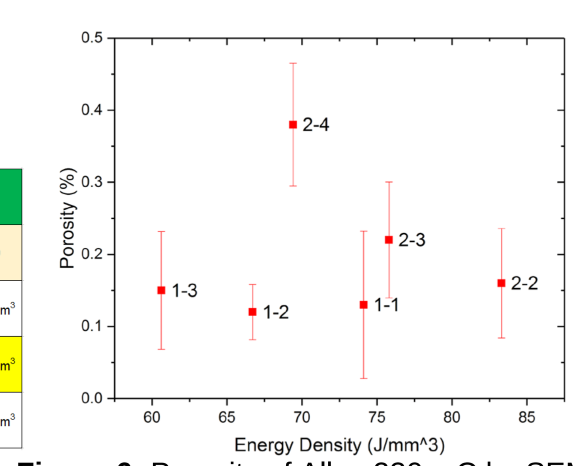

Figure 6: Porosity of Alloy 230 – C by SEM

- Alloy 230 – B created with low B, low Si, zero Mn
- Alloy 230 – C created with mid B, mid Si, zero Mn
- Crack analysis of 230 – B and 230 – C shows that the B batch has a significantly lower crack density.
- Scan speed and laser power range are narrowed down to the range that is justified in the W batch.

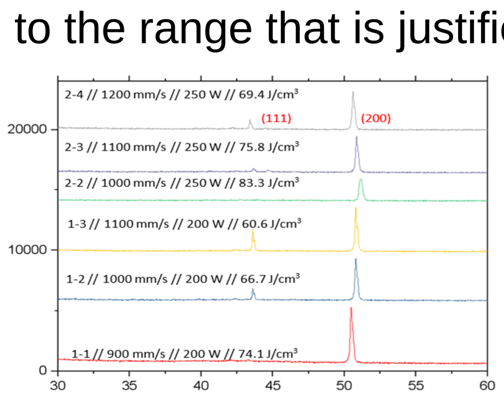

Figure 7: X-Ray Diffraction Pattern for 230 – B

- The 230 – B chemistry showed a stronger (200) peak than (111) peak.
- 230 – B chemistry has much stronger (111) peak than the 230 - W chemistry.

- There is overall reduction in crack density compared to Alloy 230 – W.
- Abundant precipitates were observed.
- The EDS map showed the even distribution of Ni, Co, Cr, Mo, Al, and B, and enrichment of W near the crack.

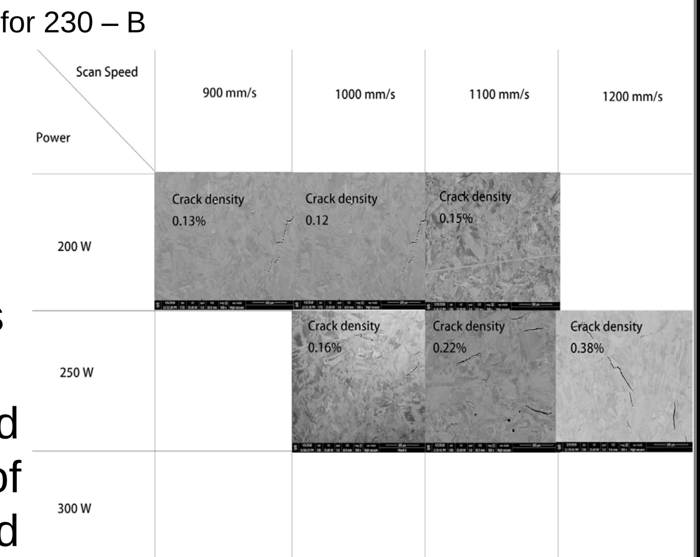

Figure 8: SEM micrograph overview corresponding to parameter matrix of samples in Alloy 230 – B.

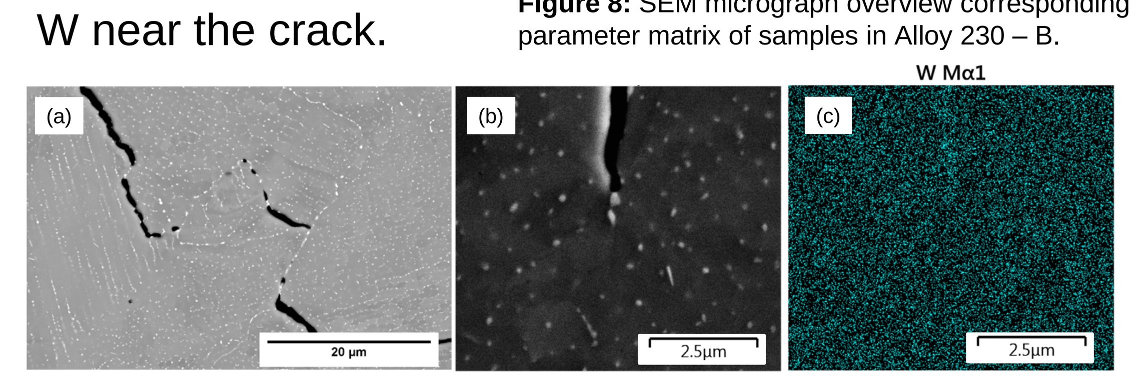

Figure 9: BSE SEM images of (a) Sample 2-3 at 4000X and (b) EDS mapping area; and (c) W intensity map across the matrix of the mapping area.

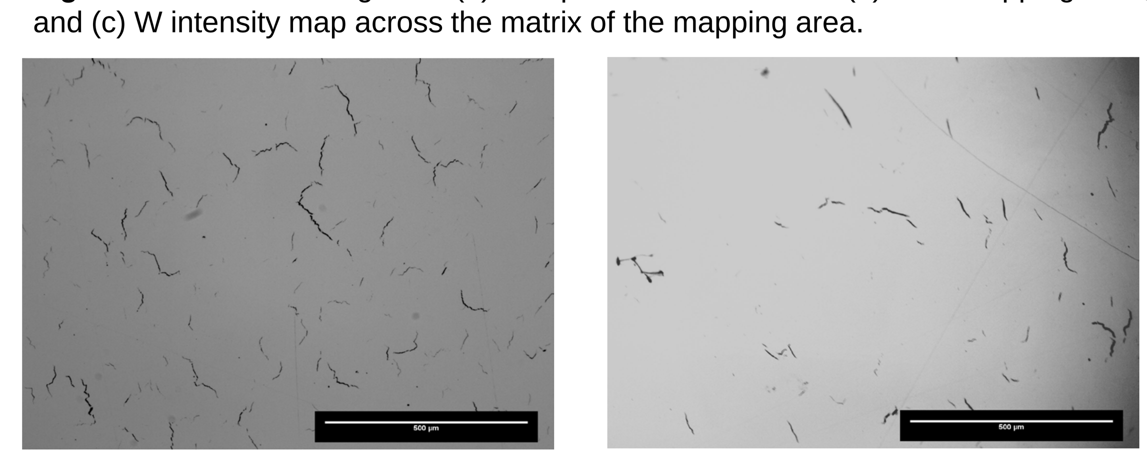

Figure 10: SEM images displaying differences in crack density of (a) Alloy 230 - W at 500X (b) Alloy 230-B at 500X

Hardness

- Alloy 230 – B (Hardness = 64.7 ± 0.92 HRA) exhibited higher hardness and lower crack density than Alloy 230 – W (Hardness = 62.5 ± 0.34 HRA)
- The suspected γ observed in the 230-B is believed to be a possible strengthening mechanism.
- The size distribution of the precipitates show the precipitates near the grain boundaries tend to be larger than the precipitates in the γ' matrix.

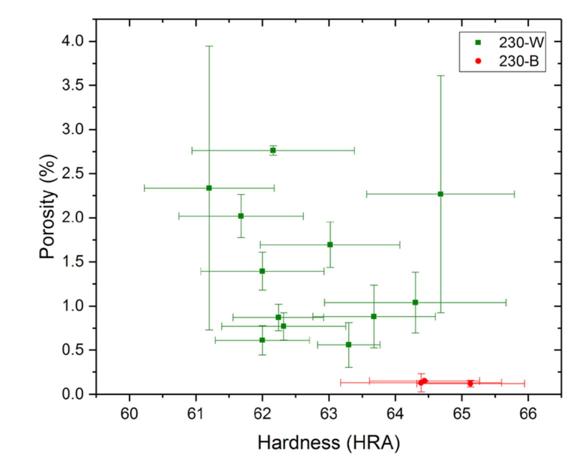

Figure 11: Porosity of 230 – W and 230 – B samples with respect to the hardness in HRA scale with error bars.

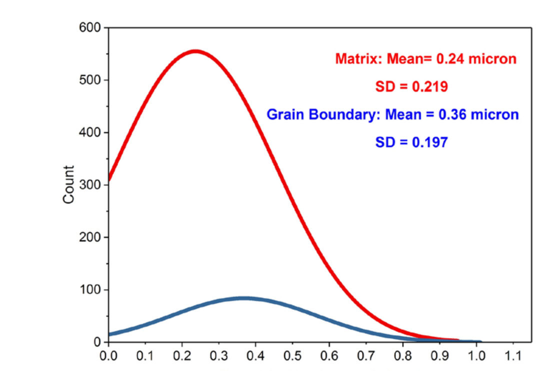

Figure 12: Precipitate size distribution in Alloy 230 –B based on and showing a normal distribution

Conclusions

- The cracks propagated along the grain boundaries as intergranular cracking. Two possible cracking mechanisms are:
  - Thermal stress on brittle γ' phase during printing/cooling of the alloys
  - Grain boundary liquation from the low melting point in the grain boundaries propagating along the γ phase
    - The W segregation near the cracks is an indication for the liquation mechanism.
- Alloy 230 – W exhibited cracking and low hardness most likely due to chemistry.
- Studies of Alloy 230 – B and Alloy 230 – C suggest that a low Si and Mn composition (Alloy 230 – B) may lead to less cracking.
- Alloy 230 – B showed an overall smaller porosity than Alloy 230 – W, thought to be caused by the differences in Si and Mn.
- Alloy 230 - B contains regular γ precipitates.

Recommendations

1. TEM and WDS can be conducted to understand the chemical composition of the precipitates and matrix and to categorize the morphological structure of precipitates.

2. Perform EBSD to analyze the effects of texture on the properties and morphology of samples.

3. Simulate a Ni-Cr-W ternary phase diagrams to have a better understanding on the phase stability of the alloys.

References

[1] Yap, C. Y., et al. "Review of selective laser melting: Materials and applications." Applied Physics Reviews 2.4 (2015): 041101.

[2] Bauer, T., Dawson, K., Spierings, A.B., Wegener, K., (N/A).. *Microstructure and Mechanical Characterization of SLM processed Haynes 230.*